Coherent Optical Phonon Oscillations in Bulk GaN Excited by Far below the Band Gap Photons

K. J. Yee, K. G. Lee, E. Oh, and D. S. Kim*
Department of Physics, Seoul National University, Seoul 151-747, Korea

Y. S. Lim
Department of Applied Physics, KonKuk University, Chungju, Chungbuk 380-701, Korea
(Received 18 September 2001; published 19 February 2002)

We report on generation of coherent optical phonon oscillations in 150 μm thick bulk GaN. With photon energy far below the band gap, the generation mechanisms of coherent phonon modes of A_1(LO), high- and low-frequency E_2 are revealed to be the impulsive stimulated Raman scattering. We find that one among the two degenerate E_2 modes is selectively detected with a proper choice of probe polarization. Dephasing times range from 1.5 to 70 ps for different modes, and phonon–three-photon absorbed carrier interactions are compared between the A_1(LO) and the E_2 mode.

DOI: 10.1103/PhysRevLett.88.105501 PACS numbers: 63.20.–e, 78.30.Fs, 78.47.+p

With the continuing development of femtosecond pulse lasers, generation and detection of high frequency coherent phonon modes have become possible [1–3]. Recently, coherent control of phonon oscillations was realized, and the effective femtosecond x-ray switch based on coherent phonons has been suggested [4,5]. Coherent optical phonons were studied in various materials [6,7], and coherent phonon-polariton dynamics was studied using below band-gap photons in semiconductors and ferroelectrics [8–10].

Recently, wide band gap semiconductors such as GaN, InGaN, and ZnO have attracted much attention because of their potential for development of optoelectronic devices in the blue and ultraviolet spectral regions and high temperature electronics. The frequencies and dispersion curves of phonon modes for group III nitride materials have been intensively studied by cw-Raman and inelastic x-ray scatterings [11–13]. The scattering rates of the A_1(LO) and E_1(LO) phonon modes were revealed by time-resolved anti-Stokes Raman scattering for wurtzite GaN [14,15].

Large acoustic lattice vibrations were reported in GaN/InGaN quantum well structures [16,17], but there has never been any report of coherent optical phonon generations in GaN materials. Noting that the vast majority of coherent phonon generations in semiconductors were achieved using above the band gap excitation, this shortage was most likely due to the following difficulties: (1) the high frequency of GaN optical phonons requires sub-20 femtosecond (fs) pulses (2) generating these short pulses with photon energies above the band gap of GaN is rather tricky.

In this Letter, we report the first observation of coherent optical phonon oscillations in GaN. Polarization dependencies demonstrate that the coherent phonon generation is through the impulsive Raman scattering. Separation of two degenerate E_2 modes is achieved in the detection process. Dephasing times are directly measured for the three observed modes, which range from 1.5 to 70 ps. Although we are exciting far below the band gap, we show that we can still see the direct signature of phonon dephasing through the generation of carriers via three-photon absorption. Physics of coherent phonon excitation in semiconductors through below the band gap is rich because we can investigate pure phonon dynamics and carrier-related phonon dynamics simultaneously. Our technique can easily be extended to other wide band gap materials such as ZnO or ZnSe.

Pump-probe and time-resolved electro-optic sampling experiments were performed in transmission geometry at room temperature. Transform-limited 15 fs pulses with center wavelengths near 800 nm were obtained from a Kerr-lens mode-locked Ti:sapphire laser. A fast-scanning shaker was used to detect the time derivative of transmission changes. The sample is freestanding 150-μm-thick GaN grown by the hydride vapor phase epitaxy (HVPE) method. The growth direction is parallel to the c axis of GaN.

Figure 1a shows the experimental geometries. Polarization of the probe beam is set to be parallel to a cleaved axis ($[2\bar{1}\bar{1}0]$), and the angle φ of pump polarization is measured from that axis. The time derivatives of transmission changes obtained in the pump probe with different pump polarizations are shown in Fig. 1b. Beatings between two frequency components are observed for $\varphi = 0°$ and 90°, but only one phonon mode exists for $\varphi = 45°$. Indeed, as Fig. 1c shows, the Fourier transformed intensities reveal both the A_1(LO) and the high frequency E_2 modes. The pump polarization dependence of phonon amplitudes is depicted in Fig. 1d for both modes. The amplitude of the A_1 mode for which the displacement is along the c axis is almost independent of pump polarization, unlike the E_2 mode vibrating in the plane perpendicular to the c axis.

As the photon energy is much smaller than the fundamental band gap of GaN, carrier generation is not directly involved for coherent phonon excitations. The most probable generation mechanism is the impulsive stimulated Raman scattering (ISRS) [18,19]. In the impulsive stimulated Raman scattering, both the incoming and outgoing photon polarizations that "surround" the Raman tensor

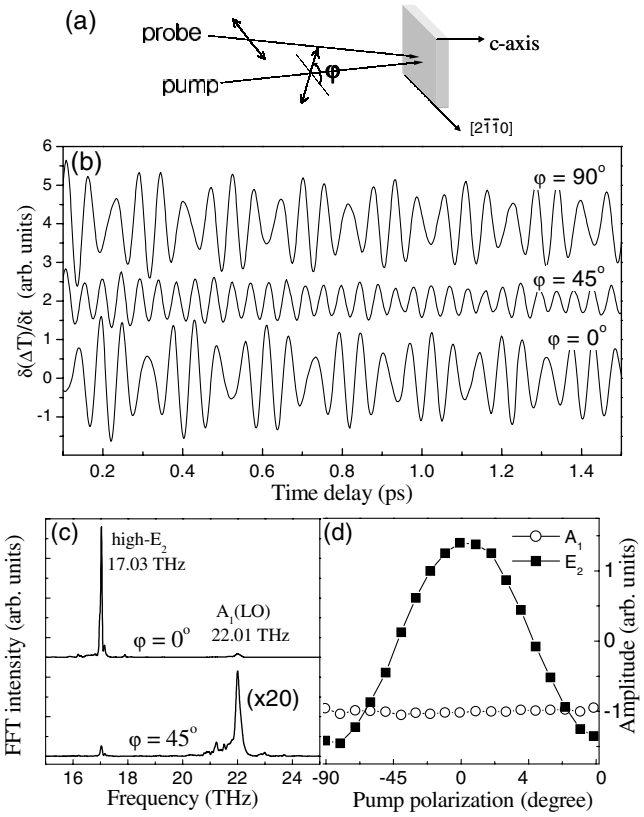

FIG. 1. (a) Experimental geometry. The polarization of the probe beam is parallel to a cleaved axis ([2$\bar{1}\bar{1}$0]) of GaN, and the pump polarization angle φ is defined from that axis. (b) Transmission changes at different pump polarizations as a function of time delay. (c) Fourier-transformed spectra of coherent phonons for $\varphi = 0°$ and $\varphi = 45°$. (d) Initial amplitudes of the E_2 and A_1(LO) modes as a function of φ.

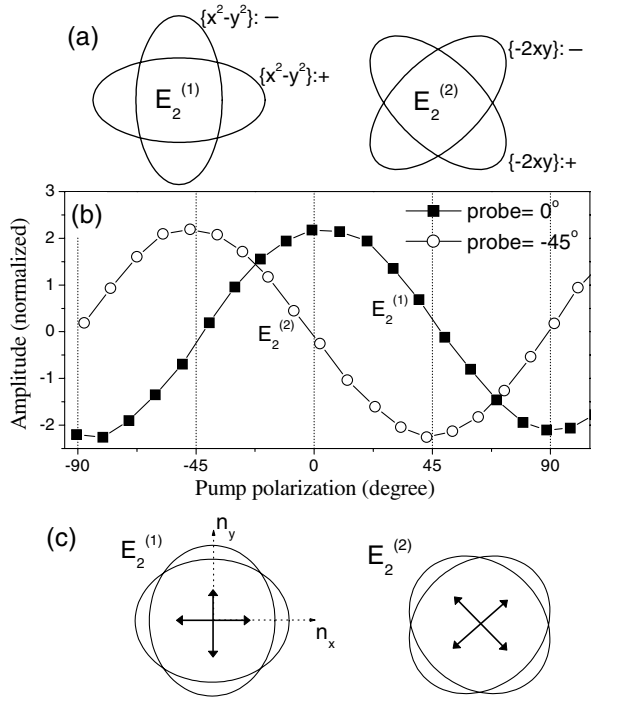

FIG. 2. (a) Schematic diagrams of phonon symmetry for the two degenerate E_2 modes. (b) Amplitudes of the E_2 modes as a function of pump polarization for probe polarization parallel to the x axis (filled squares), and for probe polarization at $-45°$ relative to the x axis (open circles). (c) Modulation of the index ellipsoids in the plane perpendicular to the c axis, induced by the E_2 modes. The both-sided arrows represent the polarization direction of the probe beam at the maximum detection efficiency for each mode.

are the same because one spectrally broad femtosecond pulse provides both the exciting photon and the Raman-stimulated photon. The Raman tensor for the A_1 mode is an eigentensor with the photon wave vector parallel to the c axis. This explains the constant amplitude with pump polarization for the A_1 mode. However, more careful considerations are needed for the E_2 mode.

Group theory predicts for wurtzite structure two degenerate E_2 modes, $E_2^{(1)}$ and $E_2^{(2)}$ with basis functions $\{x^2 - y^2\}$ and $\{-2xy\}$, respectively [20,21]. The symmetries of the E_2 modes are schematically depicted in Fig. 2a. Note that one mode is rotated 45° relative to the other. In the following analysis, we choose the rectangular axes such that $\hat{x} \parallel [2\bar{1}\bar{1}0]$, $\hat{y} \parallel [0\bar{1}10]$, and $\hat{z} \parallel [0001] \parallel \hat{c}$. The Raman tensors that determine the selection rules of the phonon excitation are given as follows for the two E_2 modes:

$$E_2^{(1)} = \begin{pmatrix} d & 0 & 0 \\ 0 & -d & 0 \\ 0 & 0 & 0 \end{pmatrix}, \qquad E_2^{(2)} = \begin{pmatrix} 0 & -d & 0 \\ -d & 0 & 0 \\ 0 & 0 & 0 \end{pmatrix}. \tag{1}$$

In the ISRS mechanism, the scattering amplitudes S as a function of pump polarization angle φ are obtained from the tensors.

$$S(E_2^{(1)}) \propto d \times \cos(2\varphi), \qquad S(E_2^{(2)}) \propto -d \times \sin(2\varphi). \tag{2}$$

For the excited E_2 mode, the total intensity is independent of the pump polarization ($\cos^2 2\varphi + \sin^2 2\varphi = 1$), and the symmetry of the linear superposition of the $E_2^{(1)}$ and $E_2^{(2)}$ modes follows the pump polarization. We find that the pump polarization dependence for the E_2 mode amplitude, shown in Fig. 1d, is entirely consistent with the $\cos 2\varphi$ dependence of the $E_2^{(1)}$. For more study we changed the probe polarization such that it is $-45°$ relative to the x axis. In this case, the initial amplitude of the E_2 mode, shown as hollow circles in Fig. 2b, is consistent with the $\cos 2\varphi$ dependence of the $E_2^{(2)}$ mode. To gain further insight into this dependence, it is necessary to understand the electro-optic effect in the detection process.

Electric fields, which accompany phonon oscillations, modulate the optical susceptibility through the first-order electro-optic effect. From the Pockels tensor of the wurtzite structure [22], we find that the change of the refractive index ellipsoid occurs in the same direction as the phonon-induced electric field ($E_{x,y}$) in the x-y plane, and the refractive index change ($\Delta n_{x,y}$) is approximated as

follows:

$$\Delta n_{x,y} = -\frac{1}{2}\,\frac{r_{51}^2 n_o^2 n_o^5}{n_e^2 - n_o^2}\,(E_{x,y})^2, \qquad (3)$$

where n_o, n_e, and r_{51} are ordinary and extraordinary refractive indices and the electro-optic coefficient of GaN. The corresponding distortions of the spherical index ellipsoids are shown for the E_2 modes in Fig. 2c. In our pump-probe geometry, the probe beam detects the change of the index ellipsoid along its polarization direction. Therefore, with the probe polarization parallel to the x axis or to the y axis, one can effectively detect the $E_2^{(1)}$, but the $E_2^{(2)}$ mode oscillations are not probed. Conversely, only the $E_2^{(2)}$ can be detected with polarization at $\pm 45°$ from the x axis. Thus, our results of the pump and probe polarization dependence for the E_2 modes confirm both generation mechanism of the ISRS and detection principle of the electro-optic effect.

One clear merit of the coherent phonon technique is that we can directly measure the phonon lifetimes. Figure 3 shows the dephasing of high- and low-frequency E_2 modes as well as the A_1(LO) phonon mode. The E_2 modes were obtained in transmissive electro-optic sampling (TEOS) which detects anisotropic changes of refractive indices, and thus is insensitive to the A_1 mode. The initial amplitude of the low-frequency E_2 mode is much smaller than the high-frequency one, but the mode becomes dominant at long time delays owing to its slow dephasing rates. It is interesting that there is a difference of more than 1 order between dephasing times of the high- and low-frequency E_2 modes, though the symmetry of the lattice vibrations is the same. It is most likely because the final available states for decay of the higher energy E_2 mode are much larger than that for the lower energy E_2 mode. The frequency and linewidth from the Lorentzian fitting is 4.303 and 0.0051 THz, respectively, for the low energy E_2 mode. The linewidth we measure through Fourier transform is smaller than that from earlier Raman measurements [23]. This is possibly because our long time delay scan allows very accurate measurements of lifetime, which translates into extremely good frequency resolution.

Thus far, we have discussed pure phonon dynamics at relatively low excitation density at which free carrier generation with multiphoton absorption is negligible. By focusing beams with a micro-objective lens, we could excite considerable amounts of free carriers by three-photon absorption, which is the most dominant mechanism when the photon energy is smaller than half the band gap. Shown in Fig. 4a is the relative amount of free carriers estimated from the decrease of transmission for positive time delay, which most likely occurs by free carrier absorption of the probe pulses. The estimated carrier density indeed scales with I^3, consistent with three-photon absorption.

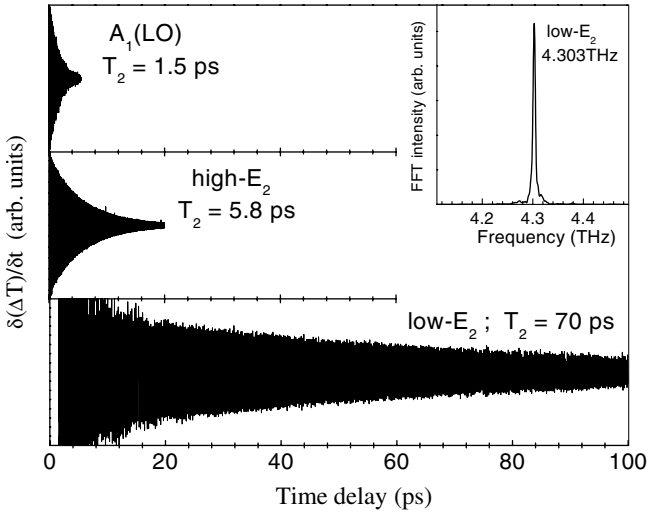

FIG. 3. Coherent phonon signals showing clear dephasing for the A_1(LO), high-E_2, and low-E_2 modes. The dephasing times 1.5, 5.8, and 70 ps were obtained from fittings for each mode. The inset is the Fourier-transformed spectra of the low-E_2 mode with the center frequency at 4.303 THz.

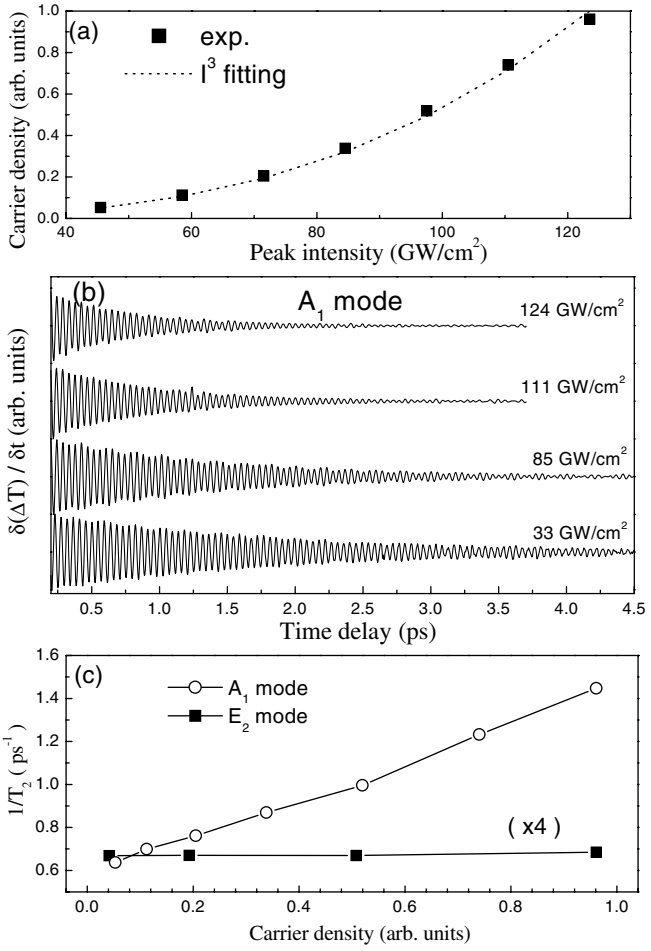

FIG. 4. (a) The estimated carrier density generated, and the dotted line is a fitting with an I^3 function. (b) Dephasing of the A_1 mode oscillations at various excitation intensities. (c) The dephasing rates of the A_1 mode (open circles), and the high-frequency E_2 mode (filled squares) as a function of a carrier density.

When electrons and holes are excited in our sample, it is expected that coherent optical phonons interact with free carriers, and this interaction can modify dephasing rates of different modes. Figure 4b shows coherent A_1 mode oscillations at various excitation densities. The dephasing time is faster by more than a factor of 2 at the highest intensity as compared with that for the lowest intensity. The scattering rates as a function of the estimated carrier density are shown in Fig. 4c. While the dephasing rate increases almost linearly with the estimated carrier density for the A_1 mode, it remains virtually constant for the E_2 mode.

In general, the dephasing rate $1/T_2$ we measure is a sum of the population decay rate $1/T_1$ and the pure dephasing rate

$$1/T_2 = 1/(2T_1) + 1/T_{2pd}\,, \tag{4}$$

where $1/T_{2pd}$ is defined as the pure dephasing rate in the absence of any population/energy decay. The factor of 2 comes from the fact that the population decay probes the energy decay, which is proportional to the square of the amplitude. Most studies that have dealt with phonon lifetimes have considered only the population decay term due to the anharmonic decay into two zone-edge acoustic phonons without consideration of any carrier-phonon interactions. The shortening of the measured dephasing time in our experiments with the increasing carrier density for the A_1 mode is likely due to the increased population decay and/or due to the pure dephasing of this mode via carrier-phonon interaction. Additional phonon population decay can be induced via heating of free carriers by coherent phonons.

If the increase of the dephasing rates were in any way owing to the increased number of coherent phonons with increasing light intensity and their collisions with each other, the E_2 mode also should have suffered the same decrease in lifetime. Since the A_1 mode has the essential characteristics of longitudinal optical phonons, strong Fröhlich interaction is expected for this mode, while the E_2 mode of dipole-forbidden nature is not expected to interact strongly with carriers. Our results are consistent with previous works [24,25] that found stronger carrier-phonon interaction for the A_1 mode compared with that for the E_2 mode for the above band gap excitation.

In summary, we studied coherent optical phonon oscillations in wurtzite GaN. With photon energy far below the band gap, coherent phonon modes of A_1(LO), high- and low-frequency E_2 were excited by the impulsive stimulated Raman scattering. We could selectively detect only one mode among the two degenerate high-frequency E_2 modes with an appropriate probe beam polarization in pump-probe experiments. We also observed the signature of carrier-phonon interaction for the A_1 phonons. Our experiments show that coherent phonon experiments using far below the band gap photons in wide-band gap semiconductors yield a variety of new phenomena, and can probe pure phonon dynamics and carrier-phonon dynamics simultaneously.

This work was supported by MOST (the National Research Laboratory Program), KOSEF (the Center for Strongly Correlated Materials Research, and Grant No. 2001-1-11100-002-3), and the National Program for Tera-level Nanodevices of the Ministry of Science and Technology as one of the 21st Century Frontier Programs.

*Electronic address: denny@phya.snu.ac.kr

[1] T. Dekorsy, G. C. Cho, and H. Kurz, in *Light Scattering in Solids VIII* (Springer, Berlin, 2000).
[2] T. K. Cheng *et al.,* Appl. Phys. Lett. **57**, 1004 (1990).
[3] T. Hasche *et al.,* Phys. Rev. Lett. **86**, 4060 (2001).
[4] M. Hase *et al.,* Appl. Phys. Lett. **69**, 2474 (1996).
[5] P. H. Bucksbaum and R. Merlin, Solid State Commun. **111**, 535 (1999).
[6] J. M. Chwalek *et al.,* Appl. Phys. Lett. **58**, 980 (1991).
[7] T. D. Krauss and F. W. Wise, Phys. Rev. Lett. **79**, 5102 (1997).
[8] T. Juhasz and W. E. Bron, Phys. Rev. Lett. **63**, 2385 (1989).
[9] H. J. Bakker *et al.,* Rev. Mod. Phys. **70**, 523 (1998).
[10] T. E. Stevens *et al.,* Science **291**, 627 (2001).
[11] V. Yu. Davydov *et al.,* Phys. Rev. B **58**, 12 899 (1998).
[12] T. Deguchi *et al.,* J. Appl. Phys. **86**, 1860 (1999).
[13] T. Ruf *et al.,* Phys. Rev. Lett. **86**, 906 (2001).
[14] K. T. Tsen *et al.,* Appl. Phys. Lett. **68**, 2990 (1996).
[15] K. T. Tsen *et al.,* Physica (Amsterdam) **272B**, 406 (1999).
[16] C. K. Sun *et al.,* Appl. Phys. Lett. **75**, 1249 (1999).
[17] J. S. Yahng *et al.* (unpublished).
[18] Y. X. Yan *et al.,* J. Chem. Phys. **85**, 5391 (1985).
[19] K. J. Yee *et al.,* Phys. Rev. Lett. **86**, 1630 (2001).
[20] Michael Tinkham, in *Group Theory and Quantum Mechanics* (McGraw-Hill, New York, 1964).
[21] A. K. Ramdas and S. Rodriguez, in *Light Scattering in Solids VI* (Springer, Berlin, 1991).
[22] F. Agullo-Lopez, J. M. Cabrera, and F. Agullo-Rueda, in *Electrooptics: Phenomena, Materials, and Applications* (Academic Press, San Diego, 1994).
[23] L. Bergman *et al.,* MRS Internet J. Nitride Semicond. Res. **4S1**, G6.65 (1999).
[24] S. J. Sheih *et al.,* Appl. Phys. Lett. **67**, 1757 (1995).
[25] A. J. Fischer *et al.,* Phys. Rev. B **56**, 1077 (1997).